The Cryosphere Discuss., doi:10.5194/tc-2016-14, 2016
Manuscript under review for journal The Cryosphere
Published: 11 February 2016

The Cryosphere Discussions
Open Access
EGU

Impacts of ikaite export from sea ice to the underlying seawater in a sea ice-seawater mesocosm

Geilfus N.-X.[1,2], Galley R. J.[1], Else B. G. T.[3], Papakyriakou T.[1], Crabeck O.[1], Lemes M.[1], Delille B.[4], Rysgaard S.[1,2,5]

[1] Centre for Earth Observation Science, Department of Environment and Geography, University of Manitoba, Winnipeg, Canada
[2] Arctic Research Centre, Aarhus University, Aarhus, Denmark
[3] Department of Geography, University of Calgary, Calgary, Canada
[4] Unité d'Océanographie Chimique, Université de Liège, Liège, Belgium
[5] Greenland Climate Research Centre, Greenland Institute of Natural Resources, Nuuk, Greenland

1. Abstract

Ikaite precipitation within sea ice could act as a significant sink for atmospheric CO_2. However, the fate of these ikaite crystals is still poorly understood. We quantify temporal inorganic carbon dynamics from initial sea ice formation from open water to its melt during a month-long experiment in a sea ice-seawater mesocosm pool. Within sea ice, ikaite precipitation and CO_2 exchange with the atmosphere were the main processes affecting inorganic carbon dynamics, while the dissolution of ikaite was the main process affecting inorganic carbon dynamics in the underlying seawater. Based on the total alkalinity (TA) and total dissolved inorganic carbon (TCO_2) within sea ice and seawater, we estimated ikaite precipitated up to 167 ± 3 µmol kg^{-1} within sea ice; up to 57% of the ikaite precipitated within sea ice was exported to the underlying seawater where it was dissolved. Ikaite export from the ice to the underlying seawater was associated with brine rejection during sea ice growth, increased sea ice vertical connectivity due to the upward percolation of seawater, and meltwater flushing during sea ice melt. The dissolution of the ikaite crystals in the water column kept the seawater pCO_2 undersaturated compared to the atmosphere in spite of increased salinity, TA, and TCO_2 associated with sea ice growth. Results indicate that ikaite export from sea ice and its dissolution in the underlying seawater can potentially hamper the effect of oceanic acidification on the aragonite saturation state ($\Omega_{aragonite}$) in fall and winter in ice-covered areas, at the time when $\Omega_{aragonite}$ is smallest.

2. Introduction

Each year, 7 Pg of anthropogenic carbon are released to the atmosphere, 29% of which is estimated to be taken up by the Oceans through physical, chemical and biological processes (Sabine et al., 2004). The

The Cryosphere Discuss., doi:10.5194/tc-2016-14, 2016
Manuscript under review for journal The Cryosphere
Published: 11 February 2016

Arctic Ocean plays a key role in these processes, taking up 5-14% of the global ocean CO_2 uptake (Bates and Mathis, 2009), primarily through primary production and surface cooling (MacGilchrist et al., 2014). However, polar ocean CO_2 uptake estimates consider sea ice an impermeable barrier, ignoring the potential role of ice-covered areas on gas exchange between the ocean and atmosphere. Recent studies have shown that sea ice covered areas participate in the variable sequestration of atmospheric CO_2 by the ocean (e.g. Papakyriakou and Miller 2011; Geilfus et al., 2012; Nomura et al., 2013; Delille et al., 2014; Geilfus et al., 2014; 2015). Studies are required to elucidate the processes responsible as well as their magnitudes both temporally and spatially.

CO_2-carbonate chemistry in sea ice and brine is heterogeneous, which leads to complex CO_2 dynamics with the potential to affect the air-sea CO_2 flux (Parmentier et al., 2013). Release of CO_2 (from sea ice to the atmosphere) has been reported during sea ice formation from open water (Geilfus et al., 2013a) and in winter (Miller et al., 2011) while uptake of CO_2 (by sea ice from the atmosphere) has been reported after sea ice melt onset (e.g. Semiletov et al., 2004; Nomura et al., 2010; Geilfus et al., 2012; Nomura et al., 2013; Geilfus et al., 2014; 2015), suggesting that the temporal cycle of sea ice formation and melt variably affects atmospheric CO_2 uptake by the ocean. Sea ice may also act as an important control on the partial pressure of CO_2 (pCO_2) in the sea surface through a sea ice pump (Rysgaard et al., 2007).

During the earliest stages of sea ice formation a small fraction of CO_2-supersaturated brine is expelled upward onto the ice surface promoting a release of CO_2 to the atmosphere (Geilfus et al., 2013a). As sea ice forms and grows thicker, salts are partly rejected from the sea ice and partly trapped within the sea ice structure, concentrated in brine pockets, tubes and channels. As a result, the physical concentration of dissolved salts, including inorganic carbon, increase within the brine and promote the precipitation of calcium carbonate crystals such as ikaite ($CaCO_3 \bullet 6H_2O$). These crystals have been reported in both natural (Dieckmann et al., 2008) and experimental sea ice (Geilfus et al., 2013b; Rysgaard et al., 2014) and have been suggested to be a key component of the carbonate system (Rysgaard et al., 2007; Delille et al., 2014).

During ikaite precipitation, TA is reduced by 2 moles due to the reduction of the bicarbonate while TCO_2 is only reduced by 1 mole (equation 1 to 3).

$$Ca^{2+} + 2HCO_3^- + 5H_2O \rightleftharpoons CaCO_3 \cdot 6H_2O + CO_2 \quad (1)$$

$$TCO_2 = [HCO_3^-] + [CO_3^{2-}] + [CO_2] \quad (2)$$

The Cryosphere Discuss., doi:10.5194/tc-2016-14, 2016
Manuscript under review for journal The Cryosphere
Published: 11 February 2016

$$TA = [HCO_3^-] + 2[CO_3^{2-}] + [B(OH^-)] + [OH^-] - [H^-] \quad (3)$$

The specific conditions leading to ikaite precipitation as well as the fate of these precipitates in sea ice are still not fully understood. Ikaite crystals may remain within the ice structure while the CO_2 formed during their precipitation is rejected with dense brine to the underlying seawater. This could be an effective process of CO_2 sequestration (Delille et al., 2014). In addition, ikaite stored in the ice matrix could become a source of TA to the near-surface ocean upon its subsequent dissolution during sea ice melt (Rysgaard et al., 2007; 2009).

The main fluxes of CO_2 and TCO_2 are driven by brine rejection to the underlying seawater and incorporated into intermediate and deep-water masses in the Arctic (Semiletov et al., 2004; Rysgaard et al., 2007, 2009) or below sea ice in ice tank studies by Killawee et al., (1998) and Papadimitriou et al., (2004). As sea ice thickens, reduced near-surface ice temperatures result in reduced brine volume content, increased brine salinity and increased solute concentration in the brine. In the spring-summer, as the ice temperature increases, sea ice brine volume increases and sea ice becomes vertically permeable to liquid (Golden et al., 2007), enhancing the potential CO_2 exchange between the atmosphere, sea ice and the ocean. Eventually internal ice melt promotes brine dilution, which decreases brine salinity, TA and TCO_2, and leads to lower pCO_2 in the brine. In addition, the dissolution of ikaite decreases brine pCO_2 (Eq. 3) (Geilfus et al., 2012; 2015). These conditions all favour sea ice as a sink for atmospheric CO_2 (Nomura et al., 2010; Geilfus et al., 2012; Nomura et al., 2013; Geilfus et al., 2015). Melting sea ice promotes the stratification of surface seawater. The mixing of meltwater, that is low in TCO_2, pCO_2, and high in TA due to brine dilution and ikaite dissolution, with seawater will increase TA and decrease the pCO_2 of the underlying seawater, enhancing the air-sea CO_2 fluxes (Rysgaard et al., 2007; 2009).

Although we now have a basic understanding of the key mechanisms of carbon cycling in sea ice, significant unknowns remain. One of the major unknowns is the fate of carbon-bearing materials released from sea ice during winter. It is unclear what proportion of precipitated ikaite crystals in sea ice remain in the matrix to be released upon melt or what proportion are expelled with brine drainage during ice formation and growth. Examining the chemical signatures of the water column beneath sea ice may provide an indication of the importance of different processes. However, the signal of carbon components released from 1-2 meters of sea ice growth is difficult to detect in a water column several hundred meters deep.

The Cryosphere Discuss., doi:10.5194/tc-2016-14, 2016
Manuscript under review for journal The Cryosphere
Published: 11 February 2016

In this study, we followed the evolution of the inorganic carbon dynamics within experimental sea ice from sea ice formation from open water to melt in a sea ice-seawater mesocosm pool (~435 m^3). The benefits of this type of environment are multiple. An artificial pool equipped with a movable bridge makes it possible to collect undisturbed samples from thin growing sea ice. We gain the ability to carefully track carbon parameters in the ice, in the atmosphere, and in the underlying seawater, while growing sea ice in a large enough volume of seawater, so that conditions closely mimic the natural system. During a 3 weeks experiment, we examined the main processes responsible for major changes in the inorganic carbon system of sea ice and the underlying seawater and quantify fluxes of inorganic carbon between the atmosphere, sea ice and the water column.

3. Site description, sampling and analysis

The experiment was performed at the Sea-ice Environmental Research Facility (SERF, Fig. 1) site from 13 to 30 January 2013 at the University of Manitoba, Winnipeg, Canada. The SERF is an outdoor sea ice pool: 18.3 m by 9.1 m in surface area and 2.6 m deep exposed to ambient temperatures, winds and solar radiation (by retracting its roof). The weather conditions in the region are conducive to sea ice growth for several months every winter. Prior to the experiment, the pool is filled with artificial seawater (ASW) formulated by dissolving large quantities of various rock salts into local groundwater to mimic the major composition of natural seawater (see Rysgaard et al., (2014) for exact composition of the ASW). Sea ice is melted in the pool by circulating heated ethylene glycol through a closed-loop hose located at the bottom of the pool, allowing successive ice growth/melt experiments to be carried out during one winter. The experimental sea ice and brine exhibit similar physical and chemical properties to those observed in natural Arctic sea ice (Geilfus et al., 2013; Hare et al., 2013).

Bulk ice and seawater temperatures were recorded by an automated type-T thermocouple array fixed vertically in the pool. Seawater salinity was measured continuously using Aandera CT sensors (model 4319) located at 30, 100, 175 and 245 cm depth. The in situ seawater pCO_2 was measured every 5 sec using a Contros HydroC (resolution < 1 ppm, accuracy ± 1% of the upper range value) located at 1.3 m depth.

Air temperature and relative humidity were measured using a Vaisala HMP45C probe at a meteorological station located 2 m above the sea ice surface. Solar irradiance was continuously recorded by an Eppley Precision Spectral Pyranometer (range=0.285–2.8 μm) mounted 10 m above the sea ice

The Cryosphere Discuss., doi:10.5194/tc-2016-14, 2016
Manuscript under review for journal The Cryosphere
Published: 11 February 2016

surface. In addition, estimated photosynthetically active radiation (PAR) values at the ice bottom was recorded with Alec mkv-L PAR sensors throughout the study and ranged from 0 to 892 µmol photons m^{-2} s^{-1}.

Ice samples were collected using ceramic knives or a Kovacs Mark II coring system, depending on the ice thickness. Sampling was performed from a movable bridge to avoid walking on the ice surface and to ensure only undisturbed sites were sampled. Ice cores were collected from one end of the pool (half meter away from the edge of the pool) and at least 20 cm away from previous cored sites. Ice cores were packed in clean plastic bags and kept frozen during the 20 minutes transport to a cold laboratory and processed within a few hours.

Seawater was sampled for total alkalinity (TA) and total dissolved inorganic carbon (TCO_2) with a peristaltic pump (Cole Palmer, Masterflex-Environment sampler, equipped with PTFE tubing) through an ice core hole at the ice-water interface, at 1.25 m, and 2.5 m depth. Samples were poisoned with a solution of saturated $HgCl_2$ and stored in the dark at 4°C until analysed.

Air-ice CO_2 fluxes were measured using a Li-Cor 8100-103 chamber associated with a LI-8100A soil CO_2 flux systems. The chamber was connected in a closed loop to the IRGA with an air pump rate of 3 L min^{-1}. The measurement of pCO_2 in the chamber was recorded every sec over a 15 minute period. The flux was computed from the slope of the linear regression of pCO_2 against time (r^2>0.99) according to Frankignoulle (1988), taking into account the volume of ice or snow enclosed within the chamber. The uncertainty of the flux computation due to the standard error on the regression slope was on average ±3%.

In the cold laboratory, sea ice cores were cut into 2 cm sections using a pre-cleaned stainless steel band saw. Each section was placed in a gas-tight laminated (Nylon, ethylene vinyl alcohol and polyethylene) plastic bag (Hansen et al., 2000) fitted with a gastight Tygon tube and a valve for sampling. The plastic bag was sealed immediately and excess air was gently removed through the valve using a vacuum pump. The bagged sea ice samples were then melted in the dark at 4°C to minimize the dissolution of calcium carbonate precipitates (meltwater temperature never rose significantly above 0°C). Once melted, the meltwater mixture and bubbles were poisoned with a solution of saturated $HgCl_2$, transferred to gas-tight vials (12 ml Exetainer, Labco High Wycombe, UK) and stored in the dark at 4°C until analysed.

The Cryosphere Discuss., doi:10.5194/tc-2016-14, 2016
Manuscript under review for journal The Cryosphere
Published: 11 February 2016

Salinity was measured on bulk ice and seawater samples using a Thermo Orion 3-star with an Orion 013610MD conductivity cell and values were converted to bulk salinity (Grasshoff et al., 1983). TA was determined by potentiometric titration (Haraldsson et al., 1997) while TCO_2 was measured on a coulometer (Johnson et al., 1987). Routine analysis of Certified Reference Materials provided by A. G. Dickson, Scripps Institution of Oceanography, verified that TA and TCO_2 were analyzed within ±3 and ±2 µmol kg^{-1}, respectively. The abundance and concentration of ikaite crystals precipitated within sea ice has been estimated by inspection under microscope as the samples melted. Rysgaard et al., (2014) provide a complete description of the method used. Brine volume was estimated from measurements of bulk salinity, temperature and density according to Cox and Weeks (1983) for temperatures below -2°C and according to Leppäranta and Manninen (1988) for ice temperature within the range -2 to 0°C.

4. Results

4.1. Sea ice and seawater physical conditions

Sea ice was grown in the pool from open water on 13 January 2013 and reached a maximum thickness of 24 cm on 26 January at which point the heat at the base of the pool was turned on. On 30 January the experiment ended with the pool 20% ice-free. Three main snowfall events occurred during the experiment. The first, from 14 to 15 January, covered the sea ice surface with 1 cm of snow. The second, from 18 to 23 January, deposited 6-9 cm of snow over the entire pool. On the morning of 23 January, the snow was manually cleared off the ice surface to investigate the insulating effect of the snow on the ice temperature and the ikaite precipitation (Rysgaard et al., 2014). Finally, from noon on 24 January to 27 January, 8 cm of snow covered the entire pool until the end of the experiment on 30 January.

The air temperature at the beginning of the experiment ranged from -2°C to -26°C, which initiated rapid sea ice growth to 15 cm on 18 January (Fig. 2). During this initial sea ice growth, the sea ice was attached to the side of the pool resulting in the development of a hydrostatic pressure head that caused percolation of seawater at the freezing point upwards through the sea ice volume as the sea ice grew downwards. This results in the increase of the sea ice temperature from the bottom to the surface observed between 15 and 18 January (Fig. 2). Subsequently, the ice was cut using an ice saw around the perimeter, allowing the ice to float and a pressure release valve was installed to prevent such events (Rysgaard et al., 2014). During this period, the ice temperature oscillated between relatively warm (~ -3°C) and cold (~ -7°C) phases and the bulk ice salinity profiles were typically in C-shape with values

The Cryosphere Discuss., doi:10.5194/tc-2016-14, 2016
Manuscript under review for journal The Cryosphere
Published: 11 February 2016

ranging from 6 to 23 (Fig. 2). The underlying seawater salinity increased rapidly due to sea ice growth. From 18 to 23 January, the 9 cm snow cover insulated the ice cover from the cold atmosphere (Rysgaard et al., 2014), resulting in a fairly constant ice thickness, nearly no change in ice temperature and salinity and a small increase in the underlying seawater salinity. Once the ice surface was cleared of snow on the morning of 23 January, the ice temperature decreased throughout the entire ice thickness and the ice surface salinity increased. This rapid sea ice growth was associated with a rapid increase of the seawater salinity. Shortly after the snow clearing, the last snowfall event covered the ice surface with 8 cm of snow, reducing the effect of the cold atmosphere on the ice cover. On 26 January, the heater was activated to initiate sea ice melt. Sea ice temperature increased and became isothermal around -2°C while the bulk ice salinity decreased. The sea ice melt decreased the seawater salinity. The pool was well mixed during the whole growth phase with similar salinity and temperature observed at the four depths. However, once the heat was turned ON, the pool become stratified with respect to salinity changes, as the salinity at 30 cm depth started to diverge compare to the other depths (Fig. 2).

4.2. Carbonate system

TA and TCO_2 in seawater, noted as $TA_{(sw)}$ and $TCO_{2(sw)}$, were sampled at the sea ice-seawater interface, 1.25 and 2.5 m depth. However, as the variations of TA and TCO_2 over the 3 depths are quite small (SD = 8.75 and 4.5 µmol kg^{-1}, respectively), we consider the average concentration. During sea ice growth, $TA_{(sw)}$ increased from 2449 to 2644 µmol kg^{-1} (black line, Fig. 3a) while $TCO_{2(sw)}$ increased from 2347 to 2516 µmol kg^{-1} (black line, Fig. 3b). Once the ice started to melt, $TA_{(sw)}$ decreased to 2607 µmol kg^{-1} and $TCO_{2(sw)}$ decreased to 2461 µmol kg^{-1}. To discard the effect of salinity changes, we normalized $TA_{(sw)}$ and $TCO_{2(sw)}$ to a salinity of 33 (noted as $nTA_{(sw)}$ and $nTCO_{2(sw)}$) according to the equations 4 and 5:

$$nTA_{(sample)\,t} = \frac{TA_{(sample)\,t}}{S_{(sample)\,t}} \times 33 \quad (4)$$

$$nTCO_{2\,(sample)\,t} = \frac{TCO_{2\,(sample)\,t}}{S_{(sample)\,t}} \times 33 \quad (5)$$

where t is the time of the sampling and S the salinity of the sample (seawater or sea ice). During ice growth, $nTA_{(sw)}$ and $nTCO_{2(sw)}$ increased slightly to 2446 and 2328 µmol kg^{-1}, respectively (Fig. 3c). However, once the ice started the melt, $nTA_{(sw)}$ increased to 2546 µmol kg^{-1} and $nTCO_{2(sw)}$ increased to 2404 µmol kg^{-1}.

The Cryosphere Discuss., doi:10.5194/tc-2016-14, 2016
Manuscript under review for journal The Cryosphere
Published: 11 February 2016

The in situ pCO_2 of the underlying seawater ($pCO_{2(sw)}$) decreased from 377 to 360 ppm as the seawater temperature in the pool decreased to the freezing point. The $pCO_{2(sw)}$ then oscillated from 360 to 365 ppm during sea ice growth. One day after the heater was turned ON, the $pCO_{2(sw)}$ increased to a similar concentration as at the beginning of the experiment before decreasing to 373 ppm by the end of the experiment (Fig. 3d).

Within bulk sea ice, $TA_{(ice)}$ ranged from 300 to 1907 µmol kg^{-1} while $TCO_{2(ice)}$ ranged from 237 to 1685 µmol kg^{-1}. Both $TA_{(ice)}$ and $TCO_{2(ice)}$ exhibited C-shape profiles with higher concentrations observed at the surface and bottom layer of the ice cover (Fig. 4). The concentration of $TA_{(ice)}$ (average = 476 µmol kg^{-1}) and $TCO_{2(ice)}$ (average = 408 µmol kg^{-1}) did not show significant variability during our survey, except at the surface of the ice. A first maximum was observed on 17 January with concentration of 1907 µmol kg^{-1} for TA and 1685 µmol kg^{-1} for TCO_2. A second maximum was observed on 23 January with concentration of 1433 µmol kg^{-1} for TA and 861 µmol kg^{-1} for TCO_2. As these maxima matched the high bulk ice salinity (Fig. 2), we also normalized $TA_{(ice)}$ and $TCO_{2(ice)}$ (noted as $nTA_{(ice)}$ and $nTCO_{2(ice)}$, Fig. 4) to a salinity of 33 (according to the equations 4 and 5) to discard the effect of salinity changes and facilitate comparisons with the underlying seawater. During initial sea ice formation (up to 17 January), the concentration of both $nTA_{(ice)}$ (from 1083 to 2741, average = 1939 µmol kg^{-1}) and $nTCO_{2(ice)}$ (from 853 to 2440, average = 1596 µmol kg^{-1}) were at their minimums in the experimental time series. From 17 to 21 January, both $nTA_{(ice)}$ and $nTCO_{2(ice)}$ increased throughout the ice column (average $nTA_{(ice)}$ = 2375 µmol kg^{-1} and $nTCO_{2(ice)}$ = 2117 µmol kg^{-1}). However, from 21 January until the initial sea ice melt, $nTA_{(ice)}$ and $nTCO_{2(ice)}$ decreased in the top 5 cm of the ice cover (average $nTA_{(ice)}$ = 2125 µmol kg^{-1} and $nTCO_{2(ice)}$ = 1635 µmol kg^{-1}).

4.3. Air-ice CO_2 fluxes

The CO_2 fluxes measured at the sea ice-atmosphere interface suggest that growing sea ice exported CO_2 to the atmosphere with CO_2 fluxes ranging from 0.29 to 4.43 mmol m^{-2} d^{-1} (Fig. 5). However, as soon as the ice started to warm up and then melt, the system switched to a sink for atmospheric CO_2 with downward fluxes ranging from -1.3 to -2.8 mmol m^{-2} d^{-1}. These ranges of air-ice CO_2 exchanges are in the same order of magnitude as previous studies (also using the chamber technique) on natural sea ice in both the Arctic and Antarctica (e.g. Geilfus et al., 2014; Delille et al., 2014; Geilfus et al., 2015).

5. Discussion

The Cryosphere Discuss., doi:10.5194/tc-2016-14, 2016
Manuscript under review for journal The Cryosphere
Published: 11 February 2016

5.1. Key processes affecting the carbonate system

The dynamics of inorganic carbon in the ocean and sea ice are mainly affected by temperature and salinity changes, precipitation and dissolution of calcium carbonate, and biological activities (Zeebe and Wolf-Gladrow, 2001). During this experiment, biological activity is unlikely to have played a role as neither organic matter nor biota were purposely introduced into the pool and observed average levels of bulk ice microbial activity (1.12 x 10^{-5} g C L^{-1} h^{-1}) and algal Chl *a* (0.007 µg L^{-1}) were very low (Rysgaard et al., 2014). For this 2013 experiment, Rysgaard et al. (2014) discussed the precipitation of ikaite within the ice cover in detail, reporting high concentrations of ikaite (> 2000 µmol kg^{-1}) at the surface of the ice and ikaite precipitation up to 350 µmol kg^{-1} in bulk sea ice. This precipitation is associated with low ice temperatures, high bulk salinity and high $TA_{(ice)}$ and $TCO_{2(ice)}$ concentrations (Fig. 2 and 3).

The main processes affecting the carbonate system can be described by changes in TA and TCO_2 (Zeebe and Wolf-Gladrow, 2001). Therefore an exchange of $CO_{2(gas)}$ affects TCO_2 while TA remains constant and the precipitation-dissolution of calcium carbonate affects both TA and TCO_2 in a ratio of 2:1 (see equation 1 to 3, Fig. 6). To calculate the theoretical changes in TA and TCO_2 during the course of the experiment, we used seawater samples from 11 January, prior to sea ice formation (t=0, Table 1) as the origin point (blue circle on Fig. 6). Sea ice data are located between the theoretical calcium carbonate precipitation line and CO_2 release line (Fig. 6a) while seawater data mainly fall on the calcium carbonate dissolution line (Fig. 6b). This suggests that the carbonate system within sea ice is affected by both the precipitation of ikaite and a release of $CO_{2(gas)}$ while the underlying seawater is mainly affected by the dissolution of calcium carbonate.

5.2. Estimation of the precipitation-dissolution of ikaite

During the experiment, Rysgaard et al., (2014) estimated the precipitation of ikaite within sea ice using direct microscopic observations. However, the precipitation-dissolution of ikaite and the gas exchange are the only two processes taking place during the experiment. As illustrated in Figure 6, an exchange of CO_2 does not affect TA while the precipitation-dissolution of ikaite affect TA and TCO_2 in a ratio 2:1. Therefore, we can use TA and TCO_2 to estimate how much ikaite is precipitated or dissolved within the ice cover and the underlying seawater.

Since TA and TCO_2 are conservative with salinity, we can calculate the expected TA and TCO_2 (noted as $TA_{(ice)}^*$ and $TCO_{2(ice)}^*$ in the ice cover and $TA_{(sw)}^*$, $TCO_{2(sw)}^*$ for the water column) based on the initial

The Cryosphere Discuss., doi:10.5194/tc-2016-14, 2016
Manuscript under review for journal The Cryosphere
Published: 11 February 2016

seawater conditions ($TA_{(sw)}$, $TCO_{2(sw)}$ and $S_{(sw)}$ at t=0, Table 1) and the sample salinity (bulk sea ice or seawater) measured during the experiment:

$$TA^{*}_{(sample)\,t} = \frac{TA_{(sw)\,t=0}}{S_{(sw)\,t=0}} \times S_{(sample)\,t} \quad (6)$$

$$TCO^{*}_{2\,(sample)\,t} = \frac{TCO_{2\,(sw)\,t=0}}{S_{(sw)\,t=0}} \times S_{(sample)\,t} \quad (7)$$

where t is the time of the sampling. Within the ice cover, $TA_{(ice)}$, $TCO_{2(ice)}$ and the bulk ice salinity are averaged throughout ice at each sampling day (Fig. 7a, b, black line) while for the underlying seawater, we used the averaged $TA_{(sw)}$, $TCO_{2(sw)}$ and salinity (Fig. 2a, b, black line).

All the variations of TA observed during this experiment are due to ikaite precipitation and/or dissolution so we assume that half of the difference between $TA_{(sample)}^{*}$ and $TA_{(sample)}$ is a result of ikaite precipitation when the difference is positive (Fig. 6). A negative difference (*i.e.* $TA_{(sample)}^{*} < TA_{(sample)}$), implies that a lack of TA is observed in the sample compared to what is expected based on the observed salinity changes (Fig. 2). This suggests that ikaite crystals were either dissolved or exported out of the sample (sea ice or seawater).

5.2.1. Sea ice

The higher $TA_{(ice)}^{*}$ and $TCO_{2(ice)}^{*}$ compared to the averaged $TA_{(ice)}$ and $TCO_{2(ice)}$ (Fig. 7a, b) is expected as ikaite is precipitated (Rysgaard et al., 2014) and CO_2 released from the ice to the atmosphere (Fig. 5, 6); both processes reduce $TA_{(ice)}$ and $TCO_{2(ice)}$. We assume that half the difference between $TA_{(ice)}^{*}$ and $TA_{(ice)}$ is a result of ikaite precipitation (Fig. 7c, black dots). The precipitation of ikaite appeared to be highly variable (Fig. 7c). Ikaite precipitation was up to 167 µmol kg^{-1} (e.g. first days of the experiment) and as low as 1 µmol kg^{-1} (e.g. 19 January). A negative difference between $TA_{(ice)}^{*}$ and $TA_{(ice)}$ occurred on three occasions: 14, 20 and after the 26 January (beginning of the sea ice melt). On these occasions, the ice cover was relatively warm due to warmer atmospheric temperatures (14 January), thicker snow cover insulating the ice cover from the cold atmosphere (20 January) or when heat was turned back ON (after 26 January, Fig. 2). Relatively high sea ice temperatures likely promote ikaite dissolution in agreement with Rysgaard et al., (2014) who linked ikaite precipitation/dissolution to ice temperature. The upward percolation of seawater observed from 15 to 18 January might complicate the picture of the effect of sea ice temperature on ikaite formation. The upward percolation of seawater was in part responsible for increased ice temperatures (Fig. 2) and therefore increased brine volume in the sea ice. The increase of

The Cryosphere Discuss., doi:10.5194/tc-2016-14, 2016
Manuscript under review for journal The Cryosphere
Published: 11 February 2016

the vertical connectivity (permeability) of the network of liquid inclusions throughout the sea ice (Golden et al., 2007; Galley et al., 2015) would have allowed the export of ikaite crystals from the ice cover to the underlying seawater. However, while we calculated a negative difference between $TA_{(ice)}^{*}$ and $TA_{(ice)}$, ikaite crystals were observed by Rysgaard et al., (2014). So, we compared the direct microscopy observations by averaging the amount of ikaite precipitated throughout the ice thickness for each sampling day from Rysgaard et al., (2014) (Fig. 7c, white dots) with our estimation of the amount of ikaite based on the difference between $TA_{(ice)}^{*}$ and $TA_{(ice)}$ (Fig. 7c, black dots) and found good agreement, with some small differences likely due to methodological differences. Here, sea ice samples were melted to subsample for TA and TCO_2. During melting of the sea ice samples, ikaite crystals may have dissolved, leading to an underestimation of the total amount of ikaite precipitate in the ice. This bias is avoided during direct microscopic observation of the crystals (Rysgaard et al., 2014) if crystals are large enough to allow optical detection. However, if no crystals were observed, Rysgaard et al., (2014) assumed that no crystals were precipitated in the ice, though ikaite crystals could have been formed and then exported into the underlying seawater prior to microscopic observation of the sample. This process could explain the large difference observed during the initial sea ice formation (15-17 January) when the ice was still very thin. However, estimations from both methods show similar concentrations when the ice (i) warmed due to snowfall (18-23 January) and (ii) cooled once the snow was removed (on 23 January). Once the ice started to melt (26 January), Rysgaard et al., (2014) reported a decrease in the ikaite precipitation while in this study we reported a negative difference between $TA_{(ice)}^{*}$ and $TA_{(ice)}$, possibly indicating that ikaite dissolved in the ice or were exported to the water column.

5.2.2. Water column

The main process affecting the carbonate system in the underlying seawater is the dissolution of calcium carbonate (Fig. 6). While previous studies of ikaite precipitation within sea ice carried out over open ocean hypothesized that ikaite remained trapped within the sea ice matrix (Rysgaard et al., 2007; 2013; Delille et al., 2014), the increase of $nTA_{(sw)}$ suggests that ikaite precipitated within the ice cover can be exported towards the underlying seawater where the crystals are dissolved. According to equations 1 to 3, lower $TA_{(sw)}^{*}$ and $TCO_{2(sw)}^{*}$ compared to $TA_{(sw)}$ and $TCO_{2(sw)}$ (Fig. 3b, c) confirm the dissolution of ikaite in the underlying seawater. Therefore, half the difference between $TA_{(sw)}^{*}$ and $TA_{(sw)}$ corresponds to the amount of ikaite exported from the ice and dissolved in the underlying seawater (Fig. 8a). This amount increased over time to a maximum concentration of 66 µmol kg^{-1}.

The Cryosphere Discuss., doi:10.5194/tc-2016-14, 2016
Manuscript under review for journal The Cryosphere
Published: 11 February 2016

During the one month-long experiment, $n\mathrm{TA}_{(sw)}$ increased by 128 µmol kg^{-1} while $n\mathit{T}\mathrm{CO}_{2(sw)}$ increased by 82 µmol kg^{-1} (Fig. 3c). This suggests that 64 µmol kg^{-1} of ikaite are dissolved compared to the 66 µmol kg^{-1} estimated by the difference between $\mathrm{TA}_{(sw)}^{*}$ and $\mathrm{TA}_{(sw)}$. As a result of the 2:1 ratio of TA:$\mathit{T}\mathrm{CO}_2$, the dissolution of ikaite accounts for the entire increase of $n\mathrm{TA}_{(sw)}$ but only accounts for 64-66 µmol kg^{-1} out of the 82 µmol kg^{-1} increase in $n\mathit{T}\mathrm{CO}_{2(sw)}$. So, 16-18 µmol kg^{-1} (about 25%) of the increase of $n\mathit{T}\mathrm{CO}_{2(sw)}$ cannot be explained by the dissolution of ikaite. The increase of $n\mathit{T}\mathrm{CO}_{2(sw)}$ is more significant once the ice started to melt (26 January). As the ice melt advanced, patches of open water opened at the surface of the pool. Therefore, uptake of atmospheric CO_2 by the undersaturated seawater could take place, increasing the $\mathit{T}\mathrm{CO}_{2(sw)}$.

The dissolution of ikaite crystals could also have a strong impact on the $p\mathrm{CO}_{2(sw)}$. The water column was undersaturated compared to the atmosphere during the whole experiment (Fig. 3d). A release of CO_2, from the ice to the atmosphere was measured during sea ice growth (Fig. 5) in spite of the undersaturated $p\mathrm{CO}_{2(sw)}$. This suggests that air-ice CO_2 fluxes are only due to the concentration gradient between the ice and the atmosphere (Geilfus et al., 2012; Nomura et al., 2013) and that sea ice exchanges CO_2 with the atmosphere independently of the seawater concentration (Geilfus et al., 2014). The $p\mathrm{CO}_{2(sw)}$ is highly correlated with the seawater temperature (Fig. 2) with a rapid decrease of $p\mathrm{CO}_{2(sw)}$ during the first days of the experiment (13 to 15 January) and a relative constant $p\mathrm{CO}_{2(sw)}$ until 27 January. However, on 26 January, the heat was turned back ON affecting the seawater temperature on the same day (Fig. 2) while the impact on the $p\mathrm{CO}_{2(sw)}$ only appeared one day later (Fig. 3d). Using the equation from Copin-Montegut (1988), we normalized the $p\mathrm{CO}_{2(sw)}$ to a temperature of -1°C (noted as $np\mathrm{CO}_{2(sw)}$, blue line on Fig. 3d). The $np\mathrm{CO}_{2(sw)}$, does not show major variations during sea ice growth with values around 380 ppm. However, once the heat is turned back ON and the seawater temperature increased (on 26 January), $np\mathrm{CO}_{2(sw)}$ decreased from 383 ppm to 365 ppm. On 27 January, the $np\mathrm{CO}_{2(sw)}$ increased to 372 ppm before finally decreasing until the end of the experiment. Increase of the $np\mathrm{CO}_{2(sw)}$ happened simultaneously to the increased $p\mathrm{CO}_{2(sw)}$. The delay of reaction of $p\mathrm{CO}_{2(sw)}$ compared to the $np\mathrm{CO}_{2(sw)}$, to increased seawater temperature suggests that a process other than a the temperature change affected the $p\mathrm{CO}_{2(sw)}$. According to equation 3, the dissolution of calcium carbonate has the potential to reduce $p\mathrm{CO}_{2(sw)}$. Therefore, during sea ice growth and the associated release of salt, TA, $\mathit{T}\mathrm{CO}_2$ and ikaite crystals to the underlying seawater, ikaite dissolution could be responsible for maintaining stable $p\mathrm{CO}_{2(sw)}$ values while seawater salinity, $\mathrm{TA}_{(sw)}$ and $\mathit{T}\mathrm{CO}_{2(sw)}$ are increasing. Once the seawater temperature increased, sea

The Cryosphere Discuss., doi:10.5194/tc-2016-14, 2016
Manuscript under review for journal The Cryosphere
Published: 11 February 2016

ice started to melt releasing ikaite crystals to the underlying seawater (Fig. 2, 8a). The dissolution of these crystals may have kept the $pCO_{2(sw)}$ low and counterbalanced the effect of increased temperature.

5.3. Ikaite export from the ice cover to the water column

Export of ikaite crystals from the ice cover to the underlying seawater could be associated with brine rejection occurring during sea ice growth. Small crystals are rejected along with dense brine while the bigger crystals remain trapped within the ice matrix. The upward percolation of seawater may also facilitate the export of ikaite crystals towards the underlying seawater by increasing the vertical connectivity of the brine network within sea ice.

The amount of ikaite precipitated within the ice cover compared with the amount dissolved within the underlying seawater can be estimated from the concentration measurements (Fig. 8a) and volume of sea ice and water in the pool. We estimated that between 0 and 1.87 mol of ikaite precipitated and remained within the ice cover (Fig. 8b, Table 2), with a maximum estimation just after the snow clearing (23 January). Within the water column, 0.47 to 26.71 mol of ikaite dissolved. Once the ice started to melt (on January 26), ikaite dissolved and concentrations increased from 6.6 mol (25 January) to 20.9 and 26.7 mol (28 and 29 January). Large reductions in ikaite concentration could be due to ikaite export from the ice to the water column associated with the sea ice melt and the flushing of meltwater out of the ice. Based on the Figure 8b, ikaite precipitated in sea ice is mainly exported to the underlying seawater as from 0 to 43% of ikaite crystals remain contain within the ice cover.

5.4. Air-ice-seawater exchange of inorganic carbon, attempt of CO_2 budget.

SERF is a semi-closed system where the only possibility to gain or lose CO_2 is through gas exchange with the atmosphere. This characteristic makes it easier to track the exchange of TCO_2 in the atmosphere-sea ice-seawater system. According to Figure 7b, the ice cover always had lower $TCO_{2(ice)}$ during the experiment ($TCO_{2(ice)}^{*} > TCO_{2(ice)}$) compared to what would be expected if the CO_2 simply followed brine rejection in a conservative process (i.e. $TCO_{2(ice)}^{*}$). This could be due to different processes: (i) sea ice released CO_2 to the atmosphere, (ii) the precipitation of ikaite within sea ice decreased $TCO_{2(ice)}$ and (iii) sea ice exchanges TCO_2 with the underlying seawater. To estimate the amount of TCO_2 exchanged during this experiment, we convert our units to moles, using the sea ice (and seawater) thickness (in meter) and density (in kg/m^3) and the pool dimension (in meter). The total amount of $TCO_{2(ice)}$ lost from the ice cover, estimated by the difference between $TCO_{2(ice)}^{*}$ and $TCO_{2(ice)}$, ranged from 0.11 to 6.02 mol

The Cryosphere Discuss., doi:10.5194/tc-2016-14, 2016
Manuscript under review for journal The Cryosphere
Published: 11 February 2016

379 (average 2.38 mol, Fig. 8, black dots). The maximum outgassing happened on 15-16 January, during
380 initial sea ice growth and from 23 to 25 January, during ice cooling due to snow removal. The exchange
381 of CO_2 between the ice and the atmosphere is known (Fig. 5) and ranged from 0.01 to 0.42 mol during
382 sea ice growth and from -0.15 to -0.93 mol during sea ice melt (Fig. 9, white triangles). On average, over
383 the duration of the experiment, the ice cover released 0.08 mol of CO_2 to the atmosphere. As we know
384 how much ikaite is contained within the ice cover (Fig. 8b), we can estimate how much TCO_2 is exported
385 from the ice to the underlying seawater (Fig. 9, blue triangles) by subtracting the air-ice CO_2 exchange
386 and the ikaite precipitation to the total reduction of $TCO_{2(ice)}$ observed within the ice cover (Fig. 9, black
387 dots). The ice-seawater TCO_2 exports ranged from 0.2 to 3.98 mol, confirming that sea ice primarily
388 exports TCO_2 to the underlying seawater (up to 99%), as suggested by Sejr et al., (2011). Between the
389 beginning and the end of the experiment, sea ice exported 2.8 mol of TCO_2 to the underlying seawater
390 (Fig. 9), which corresponds to a $TCO_{2(sw)}$ increase of 71 µmol kg^{-1} considering the average sea ice
391 thickness and density during the experiment and the volume of the pool. However, $TCO_{2(sw)}$ increased by
392 115 µmol kg^{-1} over the whole experiment (Fig. 3c), leaving an increase of 44 µmol kg^{-1} in the $TCO_{2(sw)}$
393 that cannot be explained by the sea ice-seawater exchange of TCO_2. As the ice melt advanced, patches of
394 open water opened at the surface of the pool. As the seawater pCO_2 was undersaturated compared to the
395 atmosphere (Fig. 3d), uptake of CO_2 could take place. Considering the pool volume, the 44 µmol kg^{-1}
396 increase of $TCO_{2(sw)}$ could be explained by an air-sea water CO_2 uptake of 5.1 mmol m^{-2} d^{-1} over 3 days
397 of sea ice melt in a 20% ice free pool. High air-sea gas exchanges rates have been observed over partially
398 ice-covered seas (Else et al., 2011; 2013) and is predicted by models that account for additional sources
399 of turbulence generated by the presence of sea ice (Loose et al., 2014).

400 The design of the experiment allowed for constrained measurement of inorganic carbon fluxes between
401 sea ice and the water column, which is not possible in a natural environment where large volume,
402 convection processes alter the underlying seawater making it more complicated to identify changes. It is
403 therefore theoretically possible to calculate a CO_2 budget from the initial sea ice growth to melt. Our
404 attempt to build up a CO_2 budget will only be based on the growing phase of the experiment because only
405 two days of data for the melt phase are available and the experiment stopped while the pool was 20% ice-
406 free (Rysgaard et al., 2014; Else et al., 2015). At the initial seawater condition on 11 January (origin
407 point, t=0), the pool contained 1040.9 mol of $TCO_{2(sw)}$ while on the last day of sea ice growth (last day
408 with seawater and sea ice data collected prior to heating), the seawater in the pool contained 1017.3 mol

The Cryosphere Discuss., doi:10.5194/tc-2016-14, 2016
Manuscript under review for journal The Cryosphere
Published: 11 February 2016

409 of $TCO_{2(sw)}$ (Table 2). This suggest that 23.6 mol of TCO_2 were transferred from the water column to
410 either the ice cover or the atmosphere. However, the TCO_2 content within the ice cover at the end of the
411 growing phase was 15.6 mol and the ice cover released 3.1 mol of CO_2 to the atmosphere (Table 2).
412 Therefore, on the 23.6 mol of TCO_2 exchanged from the water column, 4.9 mol are unaccounted for. A
413 possible explanation comes from the air-ice CO_2 fluxes. The air-seawater CO_2 fluxes are unknown until
414 the ice started to grow (13 January), but the chamber technique to estimate the air-ice CO_2 fluxes may
415 underestimate the exchange of CO_2. Another explanation could come from our estimation of the coupled
416 sea ice/seawater thickness. During our calculations, we assumed a homogeneous sea ice cover over the
417 whole pool. However, an error of 1 cm in the estimation of the seawater depth corresponds to the 4.9 mol
418 of TCO_2 missing in our budget. Using the seawater conditions at the end of the experiment, a layer of
419 1cm of seawater in the pool contains 4.21 mol of TCO_2, making it difficult to close our budget.

420 **5.5. Impact of sea ice growth on aragonite saturation state of Arctic Ocean in the context of ocean**
421 **acidification**

422 The Arctic Ocean is a region where calcifying organisms are particularly vulnerable to ocean
423 acidification since low temperature and low salinity decrease the carbonate saturation state. As a result
424 several area of the Arctic Ocean are already undersaturated with respect to aragonite (Chierici and
425 Fransson 2009; Yamamoto-Kawai et al., 2009; *Bates et al.,* 2011]. This undersaturation is enhanced in
426 winter as the temperature decreases and pCO_2 increases as a result of respiration. Calcifying organisms
427 might therefore be most susceptible to the effects of acidification in the winter, corresponding to annual
428 minimum in aragonite saturation ($\Omega_{aragonite}$). It has been suggested that sea ice retreat will enhance the
429 impact of ocean acidification by promoting surface water freshening and ventilation (Yamamoto-Kawai
430 et al., 2008; Yamamoto et al., 2012; Popova et al., 2014). However, the effect of ikaite precipitation in sea
431 ice on ocean acidification has not been addressed.

432 Figure 10 shows the evolution of $\Omega_{aragonite}$ in the water column derived from $TA_{(sw)}$ and $TCO_{2(sw)}$ and the
433 evolution of $\Omega_{aragonite}$ predicted from the change in salinity solely (i.e. using $TA_{(sw)}^*$ and $TCO_{2(sw)}^*$, noted
434 as $\Omega_{aragonite}^*$). We used the CO2sys_v2.1.xls spreadsheet [*Pierrot et al.,* 2006] with the dissociation
435 constants from Goyet and Dickson (1989) and others constants advocated by DOE (1994).

436 During ice growth, salt rejection by sea ice decreases pH and increases $\Omega_{aragonite}$. This alleviates the
437 effect of decreased temperature. However, the effect of ikaite rejection and subsequent change in TA

The Cryosphere Discuss., doi:10.5194/tc-2016-14, 2016
Manuscript under review for journal The Cryosphere
Published: 11 February 2016

dramatically increases the $\Omega_{aragonite}$. Hence, in the present experiment, rejection of ikaite crystals by sea ice has a much stronger potential to increase $\Omega_{aragonite}$ than the rejection of salt. This suggest that under-ice ikaite rejection can potentially hamper the effect of oceanic acidification on $\Omega_{aragonite}$ in fall and winter in ice covered areas at the time when $\Omega_{aragonite}$ reaches its minimum. Ice formation may therefore delay harmful effects of ocean acidification on calcifying organisms in the Arctic Ocean, by increasing $\Omega_{aragonite}$ at the critical winter period when $\Omega_{aragonite}$ reaches its minimal values. As a corollary, ice removal acts to impede the effect of ikaite rejection and therefore promote decreased $\Omega_{aragonite}$. This calls for taking into account under-ice ikaite rejection in modeling predictions of the consequences of ocean acidification in the Arctic Ocean in the context of sea ice rapid shrinking.

6. Conclusion

During a month-long experiment in a sea ice-seawater mesocosm pool, we quantified the evolution of inorganic carbon dynamics from initial sea ice formation from open water to its melt. In sea ice, ikaite precipitation and CO_2 exchange with the atmosphere were the main processes affecting inorganic carbon while dissolution of ikaite was the main process affecting inorganic carbon in the underlying seawater.

Based on our analysis of TA and TCO_2, estimation of ikaite precipitation within sea ice here (up to 167 ± 3 µmol kg^{-1}) matched previous estimates from Rysgaard et al., (2014) based on microscopically observed values. However, on three occasions, the ice cover in this experiment was enriched in TA, suggesting that ikaite crystals were missing from the ice cover, either having been dissolved or exported from the ice to the underlying seawater. In the underlying seawater, a net increase of $nTA_{(sw)}$ was observed (up to 66 µmol kg^{-1}), suggesting that a portion of the ikaite crystals precipitated within sea ice were exported to the underlying seawater and then dissolved.

Rysgaard et al., (2007) suggested that ikaite precipitation within sea ice could act as a significant sink for atmospheric CO_2. However, to act as a sink for atmospheric CO_2, ikaite crystals must remain in the ice structure while the CO_2 produced by their precipitation is expelled with dense brine rejection and entrained in deep seawater (Delille et al., 2014). We estimate up to 43 % of the ikaite precipitated in the ice remained trapped in the ice structure. The rest is exported to the underlying seawater along with brine rejection or due to the increased vertical connectivity within sea ice during events of upward seawater percolation due to hydrostatic pressure. During sea ice melt, ikaite could also be flushed downward out of the ice cover along with meltwater.

Ikaite export from sea ice and its dissolution had a strong impact on the underlying seawater. In this semi-closed system, sea ice growth increased the seawater salinity, $TA_{(sw)}$, and $TCO_{2(sw)}$. In spite of those increases, the pCO_2 of the underlying seawater remained undersaturated compared to the atmosphere. We conclude that ikaite dissolution within the water column is responsible the seawaters' continual pCO_2 undersaturation. In addition, we project that dissolution of ikaite crystals exported from sea ice in the underlying seawater can potentially hamper the effect of oceanic acidification on $\Omega_{aragonite}$ in fall and winter in ice-covered areas at the time when $\Omega_{aragonite}$ is smallest.

7. Acknowledgments

We gratefully acknowledge the contributions of the Canada Excellence Research Chair (CERC) and Canada Research Chair (CRC) programs. Support was also provided by the Natural Sciences and Engineering Research Council (NSERC), the Canada Foundation for Innovation and the University of Manitoba. RJG thanks the NSERC Discovery Grant program. B.D. is a research associate researcher of the F.R.S.-FNRS. This work is a contribution to the ArcticNet Networks of Centre of Excellence and the Arctic Science Partnership (ASP) asp-net.org.

8. References

Bates, N. R., Cai, W. J., and Mathis, J. T.: The ocean carbon cycle in the western Arctic Ocean: Distributions and air-sea fluxes of carbon dioxide, Oceanography, 24, 186-201, 2011.

Bates, N. R. and Mathis, J. T.: The Arctic Ocean marine carbon cycle: evaluation of air-sea CO_2 exchanges, ocean acidification impacts and potential feedbacks, Biogeosciences, 6, 2433-2459, 2009.

Chierici, M. and Fransson, A.: Calcium carbonate saturation in the surface water of the Arctic Ocean: undersaturation in freshwater influenced shelves, Biogeosciences, 6, 2421-2431, 2009.

Copin Montégut, C.: A new formula for the effect of temperature on the partial pressure of carbon dioxide in seawater, Marine Chemistry, 25, 29-37, 1988.

Cox, G. F. N. and Weeks, W. F.: Equations for determining the gas and brine volumes in sea-ice samples, Journal of Glaciology, 29, 306 - 316, 1983.

Delille, B., Vancoppenolle, M., Geilfus, N.-X., Tilbrook, B., Lannuzel, D., Schoemann, V., Becquevort, S., Carnat, G., Delille, D., Lancelot, C., Chou, L., Dieckmann, G. S., and Tison, J.-L.: Southern Ocean CO_2 sink: The contribution of the sea ice, Journal of Geophysical Research: Oceans, 119, 6340-6355, 2014.

495 Dieckmann, G. S., Nehrke, G., Papadimitriou, S., Gottlicher, J., Steininger, R., Kennedy, H., Wolf-Gladrow, D.,
496 and Thomas, D. N.: Calcium carbonate as ikaite crystals in Antarctic sea ice, Geophysical Research Letters, 35,
497 2008.

498 DOE (Ed.): Handbook of methods for the analysis of the various parameters of the carbon dioxide system in sea
499 water, 1994.

500 Else, B. G. T., Galley, R. J., Lansard, B., Barber, D. G., Brown, K., Miller, L. A., Mucci, A., Papakyriakou, T.
501 N., Tremblay, J. E., and Rysgaard, S.: Further observations of a decreasing atmospheric CO_2 uptake capacity in
502 the Canada Basin (Arctic Ocean) due to sea ice loss, Geophysical Research Letters, 40, 1132-1137, 2013.

503 Else, B. G. T., Papakyriakou, T., Galley, R., Drennan, W. M., Miller, L. A., and Thomas, H.: Wintertime CO_2
504 fluxes in an Arctic polynya using eddy covariance: Evidence for enhanced air-gas transfer during ice formation,
505 Journal of Geophysical Research, 116, 2011.

506 Else, B. G. T., Rysgaard, S., Attard, K., Campbell, K., Crabeck, O., Galley, R. J., Geilfus, N. X., Lemes, M.,
507 Lueck, R., Papakyriakou, T., and Wang, F.: Under-ice eddy covariance flux measurements of heat, salt,
508 momentum, and dissolved oxygen in an artificial sea ice pool, Cold Regions Science and Technology, 119, 158-
509 169, 2015.

510 Frankignoulle, M.: Field-Measurements of Air Sea CO_2 Exchange, Limnology and Oceanography, 33, 313-322,
511 1988.

512 Galley, R. J., Else, B. G. T., Geilfus, N. X., Hare, A. A., Isleifson, D., Barber, D. G., and Rysgaard, S.: Imaged
513 brine inclusions in young sea ice-Shape, distribution and formation timing, Cold Regions Science and
514 Technology, 111, 39-48, 2015.

515 Geilfus, N. X., Carnat, G., Dieckmann, G. S., Halden, N., Nehrke, G., Papakyriakou, T., Tison, J. L., and Delille,
516 B.: First estimates of the contribution of $CaCO_3$ precipitation to the release of CO_2 to the atmosphere during
517 young sea ice growth, Journal of Geophysical Research, 118, 2013a.

518 Geilfus, N. X., Carnat, G., Papakyriakou, T., Tison, J. L., Else, B., Thomas, H., Shadwick, E., and Delille, B.:
519 Dynamics of pCO_2 and related air-ice CO_2 fluxes in the Arctic coastal zone (Amundsen Gulf, Beaufort Sea),
520 Journal of Geophysical Research-Oceans, 117, 2012.

521 Geilfus, N. X., Galley, R. J., Cooper, M., Halden, N., Hare, A., Wang, F., Søgaard, D. H., and Rysgaard, S.:
522 Gypsum crystals observed in experimental and natural sea ice, Geophysical Research Letters, doi:
523 10.1002/2013GL058479, 2013b. 2013GL058479, 2013b.

524 Geilfus, N. X., Galley, R. J., Crabeck, O., Papakyriakou, T., Landy, J., Tison, J. L., and Rysgaard, S.: Inorganic
525 carbon dynamics of melt-pond-covered first-year sea ice in the Canadian Arctic, Biogeosciences, 12, 2047-2061,
526 2015.

527 Geilfus, N. X., Tison, J. L., Ackley, S. F., Galley, R. J., Rysgaard, S., Miller, L. A., and Delille, B.: Sea ice pCO_2
528 dynamics and air-ice CO_2 fluxes during the Sea Ice Mass Balance in the Antarctic (SIMBA) experiment -
529 Bellingshausen Sea, Antarctica, The Cryosphere, 8, 2395-2407, 2014.

530 Golden, K. M., Eicken, H., Heaton, A. L., Miner, J., Pringle, D. J., and Zhu, J.: Thermal evolution of
531 permeability and microstructure in sea ice, Geophysical Research Letters, 34, 2007.

532 Goyet, C. and Poisson, A.: New determination of carbonic acid dissociation constants in seawater as a function
533 of temperature and salinity, Deep-Sea Research Part a-Oceanographic Research Papers, 36, 1635-1654, 1989.

534 Grasshoff, K., Ehrhardt, M., and Kremling, K.: Methods of sea water analysis, Verlag Chemie, 1983. 1983.

535 Hansen, J. W., Thamdrup, B., and Jørgensen, B. B.: Anoxic incubation of sediment in gas-tight plastic bags: a
536 method for biogeochemical processes studies, Marine Ecology-Progress Series, 208, 273-282, 2000.

537 Haraldsson, C., Anderson, L. G., Hassellov, M., Hulth, S., and Olsson, K.: Rapid, high-precision potentiometric
538 titration of alkalinity in ocean and sediment pore waters, Deep sea Research I, 44, 2031-2044, 1997.

539 Hare, A. A., Wang, F., Barber, D., Geilfus, N. X., Galley, R. J., and Rysgaard, S.: pH Evolution in sea ice grown
540 at an outdoor experimental facility, Marine Chemistry, 154, 46-54, 2013.

541 Johnson, K. M., Sieburth, J. M., Williams, P. J. L., and Brandstrom, L.: Coulometric total carbon-dioxide
542 analysis for marine studies – automation and calibration, Marine Chemistry, 21, 117-133, 1987.

543 Killawee, J. A., Fairchild, I. J., Tison, J. L., Janssens, L., and Lorrain, R.: Segregation of solutes and gases in
544 experimental freezing of dilute solutions: Implications for natural glacial systems, Geochimica Et Cosmochimica
545 Acta, 62, 3637-3655, 1998.

546 Leppäranta, M. and Manninen, T.: The brine and gas content of sea ice with attention to low salinities and high
547 temperatures, Helsinki, 1988.

548 Loose, B., McGillis, W. R., Perovich, D., Zappa, C. J., and Schlosser, P.: A parameter model of gas exchange for
549 the seasonal sea ice zone, Ocean Science, 10, 17-28, 2014.

550 MacGilchrist, G. A., Garabato, A. C. N., Tsubouchi, T., Bacon, S., Torres-Valdes, S., and Azetsu-Scott, K.: The
551 Arctic Ocean carbon sink, Deep-Sea Research Part I-Oceanographic Research Papers, 86, 39-55, 2014.

552 Miller, L. A., Papakyriakou, T., Collins, R. E., Deming, J., Ehn, J., Macdonald, R. W., Mucci, A., Owens, O.,
553 Raudsepp, M., and Sutherland, N.: Carbon Dynamics in Sea Ice: A Winter Flux Time Series, Journal of
554 Geophysical Research-Oceans, 116, 2011.

555 Nomura, D., Eicken, H., Gradinger, R., and Shirasawa, K.: Rapid physically driven inversion of the air-sea ice
556 CO_2 flux in the seasonal landfast ice off Barrow, Alaska after onset surface melt, Continental Shelf Research, 30,
557 1998-2004, 2010.

558 Nomura, D., Granskog, M. A., Assmy, P., Simizu, D., and Hashida, G.: Arctic and Antarctic sea ice acts as a
559 sink for atmospheric CO_2 during periods of snowmelt and surface flooding, Journal of Geophysical Research:
560 Oceans, doi: 10.1002/2013JC009048, 2013. 6511-6524, 2013.

561 Papadimitriou, S., Kennedy, H., Kattner, G., Dieckmann, G. S., and Thomas, D. N.: Experimental evidence for
562 carbonate precipitation and CO_2 degassing during sea ice formation, Geochimica et Cosmochimica Acta, 68,
563 1749-1761, 2004.

564 Papakyriakou, T. and Miller, L.: Springtime CO_2 exchange over seasonal sea ice in the Canadian Arctic
565 Archipelago, Annals of Glaciology, 52, 2011.

566 Parmentier, F.-J. W., Christensen, T. R., Sørensen, L. L., Rysgaard, S., McGuire, A. D., Miller, P. A., and
567 Walker, D. A.: The impact of lower sea-ice extent on Arctic greenhouse-gas exchange, Nature climate change,
568 doi: DOI:10.1038/NCLIMATE1784, 2013. 195-202, 2013.

569 Pierrot, D., Lewis, E., and Wallace, D. W. R.: MS Excel Program Developed for CO_2 System Calculations,
570 Carbon Dioxide Information Analysis Center, Oak Ridge National Laboratory, U.S. Department of Energy, Oak
571 Ridge, Tennessee, doi: 10.3334/CDIAC/otg.CO2SYS_XLS_CDIAC105a, 2006. ORNL/CDIAC-105a. , 2006.

572 Popova, E. E., Yool, A., Aksenov, Y., Coward, A. C., and Anderson, T. R.: Regional variability of acidification
573 in the Arctic: a sea of contrasts, Biogeosciences, 11, 293-308, 2014.

574 Rysgaard, S., Bendtsen, J., Pedersen, L. T., Ramlov, H., and Glud, R. N.: Increased CO_2 uptake due to sea ice
575 growth and decay in the Nordic Seas, Journal of Geophysical Research, 114, 2009.

576 Rysgaard, S., Glud, R. N., Sejr, M. K., Bendtsen, J., and Christensen, P. B.: Inorganic carbon transport during
577 sea ice growth and decay: A carbon pump in polar seas, Journal of Geophysical Research-Oceans, 112, 2007.

578 Rysgaard, S., Søgaard, D. H., Cooper, M., Pu, cacute, ko, M., Lennert, K., Papakyriakou, T. N., Wang, F.,
579 Geilfus, N. X., Glud, R. N., Ehn, J., McGinnis, D. F., Attard, K., Sievers, J., Deming, J. W., and Barber, D.:
580 Ikaite crystal distribution in winter sea ice and implications for CO_2 system dynamics, The Cryosphere, 7, 707-
581 718, 2013.

582 Rysgaard, S., Wang, F., Galley, R. J., Grimm, R., Notz, D., Lemes, M., Geilfus, N. X., Chaulk, A., Hare, A. A.,
583 Crabeck, O., Else, B. G. T., Campbell, K., Sørensen, L. L., Sievers, J., and Papakyriakou, T.: Temporal
584 dynamics of ikaite in experimental sea ice, The Cryosphere, 8, 1469-1478, 2014.

585 Sabine, C. L., Feely, R. A., Gruber, N., Key, R. M., Lee, K., Bullister, J. L., Wanninkhof, R., Wong, C. S.,
586 Wallace, D. W. R., Tilbrook, B., Millero, F. J., Peng, T. H., Kozyr, A., Ono, T., and Rios, A. F.: The oceanic
587 sink for anthropogenic CO_2, Science, 305, 367-371, 2004.

588 Sejr, M. K., Krause-Jensen, D., Rysgaard, S., Sorensen, L. L., Christensen, P. B., and Glud, R. N.: Air-sea flux
589 of CO_2 in arctic coastal waters influenced by glacial melt water and sea ice, Tellus Series B Chemical and
590 Physical Meteorology, 63, 815-822, 2011.

591 Semiletov, I. P., Makshtas, A., Akasofu, S. I., and Andreas, E. L.: Atmospheric CO_2 balance: The role of Arctic
592 sea ice, Geophysical Research Letters, 31, 2004.

593 Yamamoto, A., Kawamiya, M., Ishida, A., Yamanaka, Y., and Watanabe, S.: Impact of rapid sea-ice reduction in
594 the Arctic Ocean on the rate of ocean acidification, Biogeosciences, 9, 2365-2375, 2012.

595 Yamamoto-Kawai, M., McLaughlin, F. A., Carmack, E. C., Nishino, S., and Shimada, K.: Aragonite
596 Undersaturation in the Arctic Ocean: Effects of Ocean Acidification and Sea Ice Melt, Science, 326, 1098-1100,
597 2009.

598 Yamamoto-Kawai, M., McLaughlin, F. A., Carmack, E. C., Nishino, S., and Shimada, K.: Freshwater budget of
599 the Canada Basin, Arctic Ocean, from salinity, delta O-18, and nutrients, Journal of Geophysical Research-
600 Oceans, 113, 12, 2008.

601 Zeebe, R. E. and Wolf-Gladrow, D.: CO_2 in seawater: Equilibrium, Kinetics, Isotopes, Elsevier, 2001. 2001.

The Cryosphere Discuss., doi:10.5194/tc-2016-14, 2016
Manuscript under review for journal The Cryosphere
Published: 11 February 2016

9. Table

Table 1: Seawater conditions on 11 January, before any sea ice formation (t=0)

Temperature (°C)	Salinity	TA (µmol kg^{-1})	TCO_2 (µmol kg^{-1})
-1.4	33.5	2453	2341

The Cryosphere Discuss., doi:10.5194/tc-2016-14, 2016
Manuscript under review for journal The Cryosphere
Published: 11 February 2016

606 Table 2: Daily amount of TCO_2 (in mol) in the water column and sea ice, amount of ikaite precipitated

607 in sea ice (in mol) and air-ice CO_2 fluxes (mol) over the whole pool.

January (Julian Day)	$TCO_{2(sw)}$ (mol)	$TCO_{2(ice)}$ (mol)	Ikaite (mol)	Air-ice CO_2 fluxes (mol)
t=0	1040.92			
13.75	1040.10	2.38	0.17	
13.88	1044.10	2.09	0.00	
14	1043.56	2.90	0.25	0.03
14.13	1042.70	3.29	0.62	0.02
14.25	1038.17	4.91	-0.05	0.01
14.5	1037.33	4.77	0.18	0.12
14.75	1038.97	4.36	0.12	0.07
15	1037.40			0.08
15.25	1032.55	4.67	0.98	0.01
15.5	1033.97	3.89	1.58	0.07
15.92	1033.82	4.47	0.69	0.12
16.38	1024.42	7.36	1.45	0.19
16.67	1028.23	8.17	1.87	0.10
17.38	1023.33	15.48	0.29	0.22
17.67	1026.36	13.26	0.04	0.13
18.38	1029.86	11.39	0.74	0.38
18.67	1027.38	12.06	0.21	0.10
19.38	1029.15	11.13	0.01	0.23
19.67	1030.16	10.75	0.03	0.11
20.38	1028.24	10.25	-0.12	0.42
20.67	1022.43	10.36	-0.70	0.12
21.38	1025.04	10.50	0.88	0.35
23.63	1034.43	12.60	1.34	
24.38	1025.76	14.84	1.30	0.21
25.38	1017.36	15.67	1.09	0.02
25.5	1029.11			
28.67	1021.72	13.46	-0.57	-0.93
29.38	987.33	15.82	-0.56	-0.15

608

The Cryosphere Discuss., doi:10.5194/tc-2016-14, 2016
Manuscript under review for journal The Cryosphere
Published: 11 February 2016

10. Figure Captions

Figure 1: The Sea Ice Environmental Research Facility with thin sea ice covering the pond. Photo: J. Sievers.

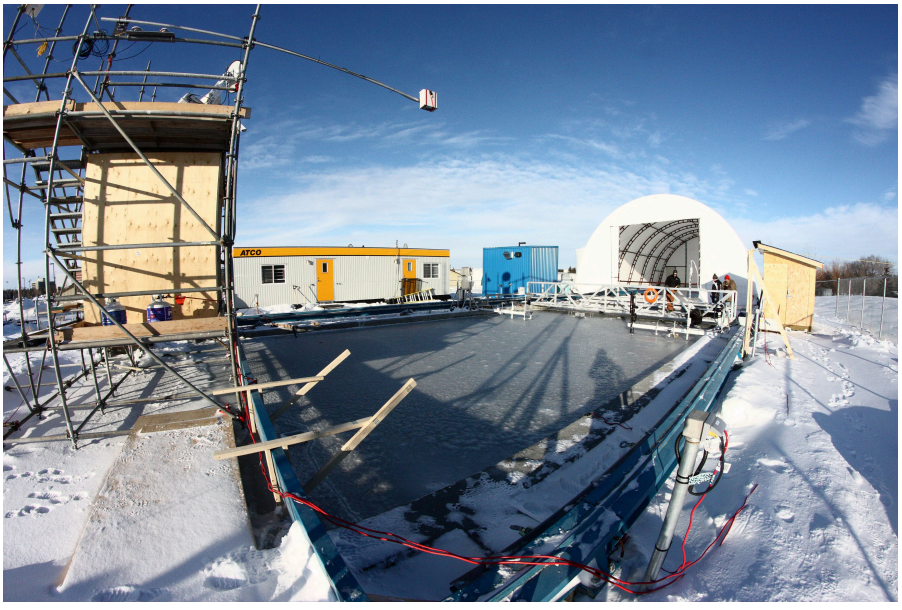

The Cryosphere Discuss., doi:10.5194/tc-2016-14, 2016
Manuscript under review for journal The Cryosphere
Published: 11 February 2016

The Cryosphere Discussions
Open Access
EGU

Figure 2: Evolution of (**A**) Air temperature (°C) at 2 m height, (**B**) snow cover (black horizontal bars) and sea ice/seawater temperature (°C), (**C**) bulk ice salinity, (**D**) seawater temperature and salinity. Measurements were performed at 30, 100, 175 and 245 cm water depths. The darker the color is, the closer to the surface. In panels (**B**) and (**C**), sea ice thickness is illustrated by black dots. Stars on panel (**B**) represent the depth at which the temperature profile are derived from. Open squares in the lower part of (**C**) mark the sampling times

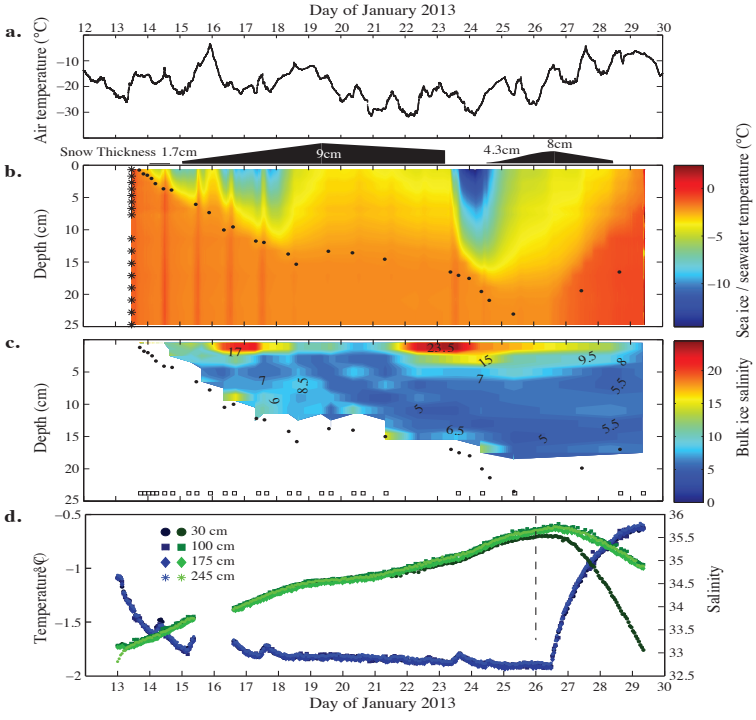

The Cryosphere Discuss., doi:10.5194/tc-2016-14, 2016
Manuscript under review for journal The Cryosphere
Published: 11 February 2016

The Cryosphere Discussions
Open Access
EGU

Figure 3: Evolution of (**A**) $TA_{(sw)}$ and $TA_{(sw)}^{*}$(µmol kg^{-1}), (**B**) $TCO_{2(sw)}$ and $TCO_{2(sw)}^{*}$ (µmol kg^{-1}), (**C**) $nTA_{(sw)}$ and $nTCO_{2(sw)}$ (µmol kg^{-1}) and (**D**) the seawater pCO_2 (µatm) measured in situ (black) and corrected to a constant temperature of -1°C (blue). In panels (**A**) and (**B**) the black line is the average over the three depths while the dotted red line is the expected concentrations according to the variation of salinity observed. The vertical black dotted line on 26 January mark when the heat was turned back ON.

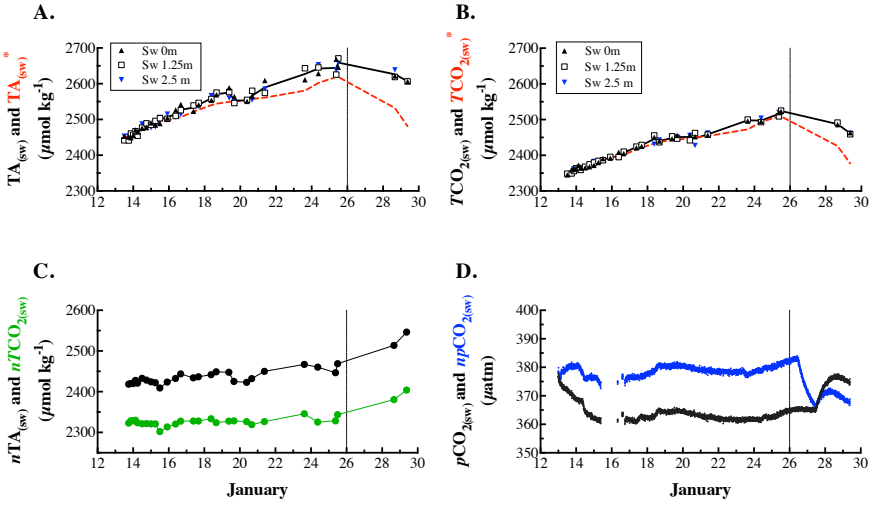

The Cryosphere Discuss., doi:10.5194/tc-2016-14, 2016
Manuscript under review for journal The Cryosphere
Published: 11 February 2016

Figure 4: Evolution of (**A**) $TA_{(ice)}$ (µmol kg^{-1}), (**B**) $TCO2_{(ice)}$ (µmol kg^{-1}), (**C**) $nTA_{(ice)}$ (µmol kg^{-1}) and (**D**) $nTCO_{2(sw)}$ (µmol kg^{-1}). Sea ice thickness is illustrated by black dots. Open squares in the lower part of (**D**) mark the sampling times.

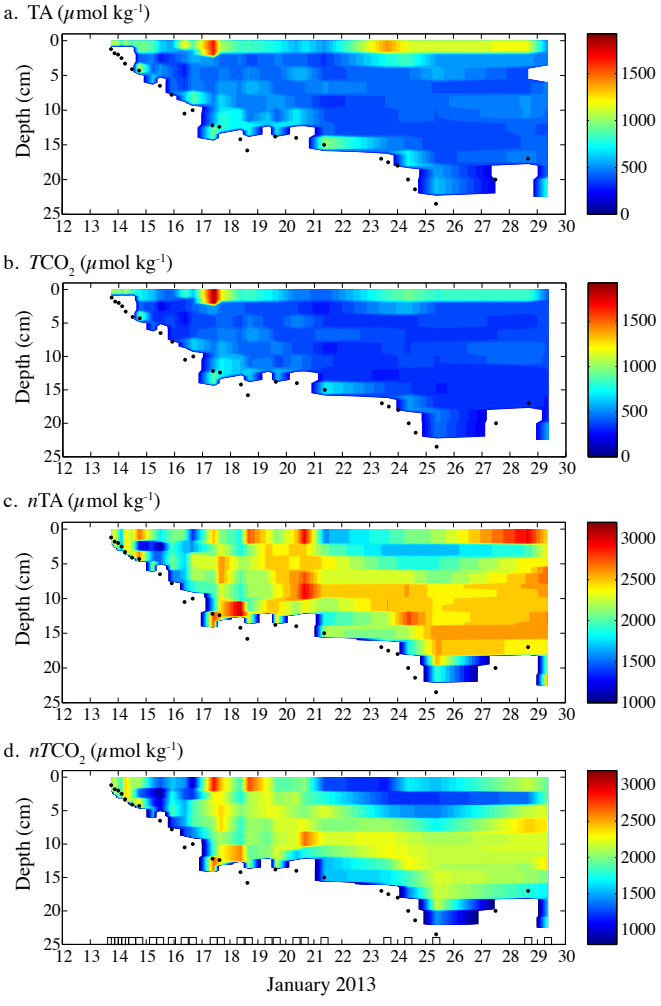

The Cryosphere Discuss., doi:10.5194/tc-2016-14, 2016
Manuscript under review for journal The Cryosphere
Published: 11 February 2016

The Cryosphere Discussions
Open Access
EGU

Figure 5: Air-ice CO_2 fluxes (mmol m^{-2} d^{-1}). The vertical black dotted line on 26 January mark when the heat was turned back ON.

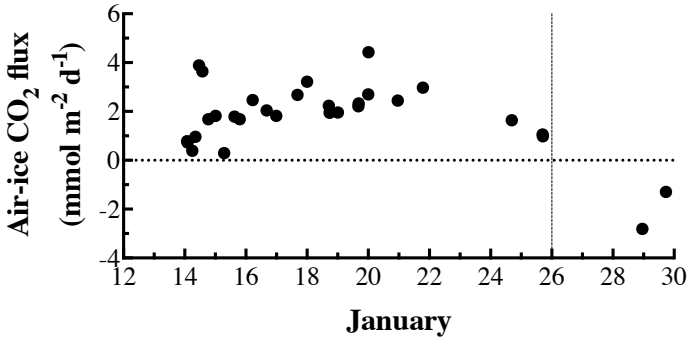

The Cryosphere Discuss., doi:10.5194/tc-2016-14, 2016
Manuscript under review for journal The Cryosphere
Published: 11 February 2016

Figure 6: (**A**) Relationship between $nTCO_2$ and nTA (µmol kg^{-1}) in bulk sea ice (white hexagons) and seawater (black dots), (**B**) Zoom on seawater data. The different dotted lines represent the theoretical evolution of nTA and $nTCO_2$ ratio following the precipitation/dissolution of calcium carbonate and release/uptake of $CO_{2(g)}$.

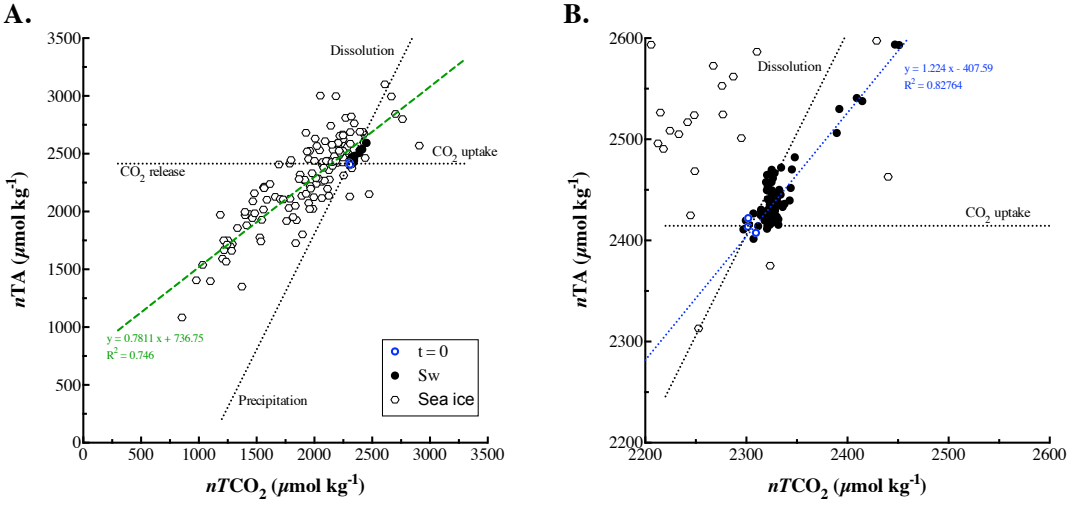

The Cryosphere Discuss., doi:10.5194/tc-2016-14, 2016
Manuscript under review for journal The Cryosphere
Published: 11 February 2016

Figure 7: Evolution of (**A**) $TA_{(ice)}$averaged throughout the ice thickness at each sampling day (black dots) and $TA_{(ice)}^{*}$ (dashed red line) (µmol kg^{-1}) and (**B**) $TCO_{2(ice)}$ averaged throughout the ice thickness at each sampling day (black dots) and $TCO_{2(ice)}^{*}$ (dashed red line) (µmol kg^{-1}), (**C**) Estimation of the ikaite precipitation/dissolution from half of the difference between $TA_{(ice)}^{*}$ and $TA_{(ice)}$ (µmol kg^{-1}). The vertical black dotted line on 26 January mark when the heat was turned back ON.

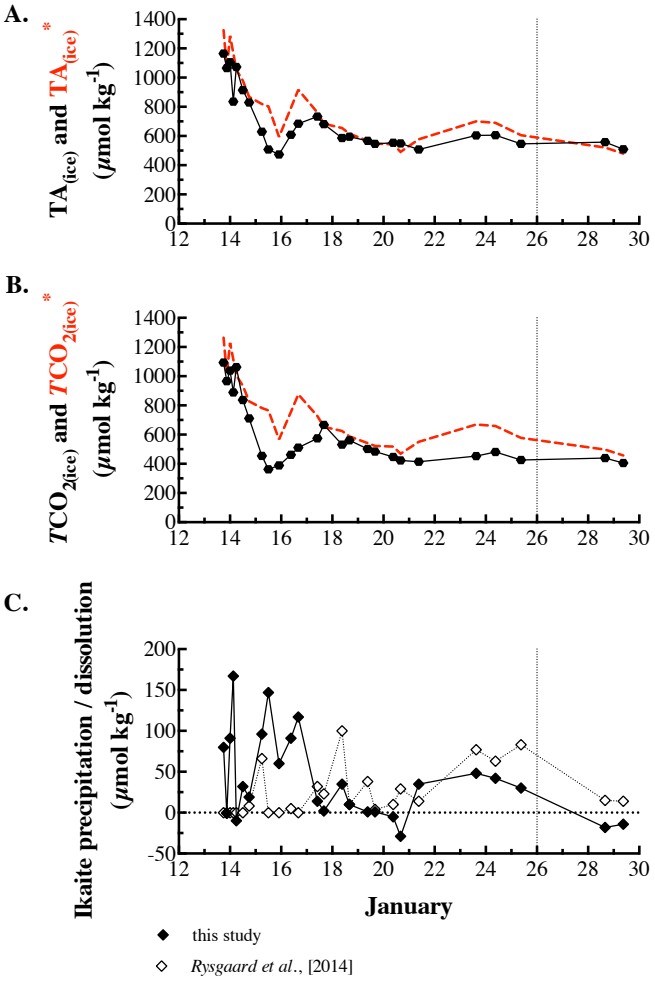

The Cryosphere Discuss., doi:10.5194/tc-2016-14, 2016
Manuscript under review for journal The Cryosphere
Published: 11 February 2016

Figure 8: Evolution of (**A**) ikaite precipitation within the ice cover in µmol kg^{-1} of sea ice (black) and ikaite dissolution within the water column in µmol kg^{-1} of seawater (blue), (**B**) amount of mole of ikaite precipitated in sea ice (black) and dissolved in the underlying seawater (blue). The vertical black dotted line on 26 January mark when the heat was turned back ON.

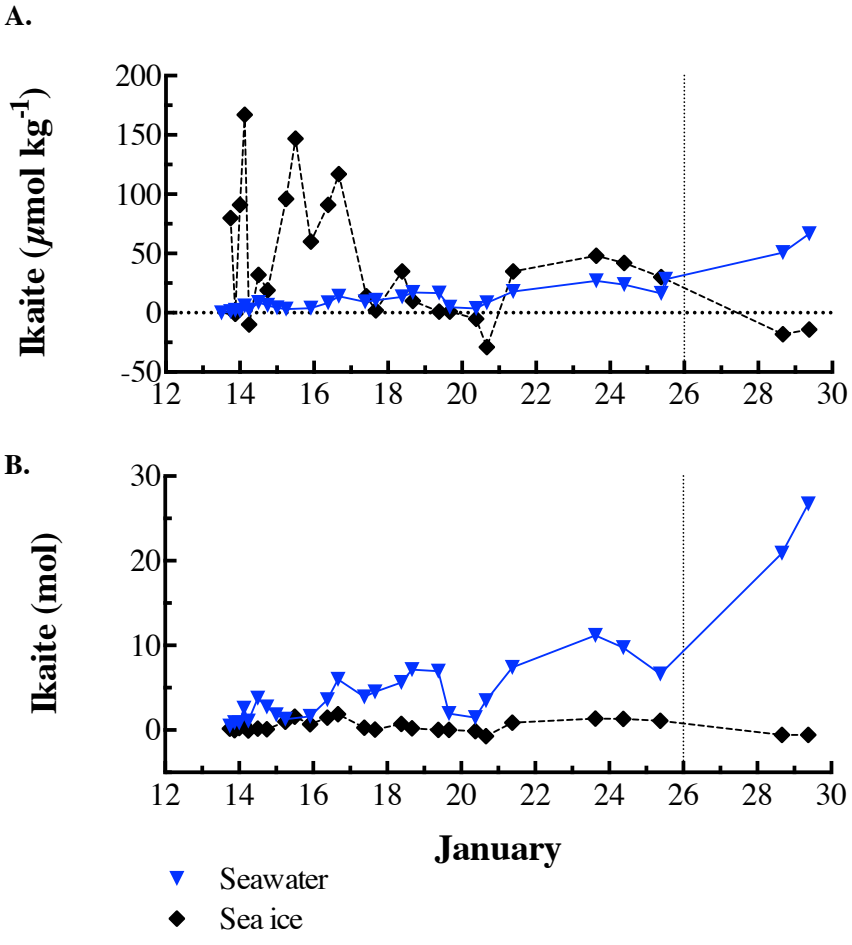

The Cryosphere Discuss., doi:10.5194/tc-2016-14, 2016
Manuscript under review for journal The Cryosphere
Published: 11 February 2016

Figure 9: Total TCO_2 exchanges by the ice cover (black dots), air-ice CO_2 fluxes (white triangle) and sea ice-water column TCO_2 exchanges (blue triangle). In mole for each day, integrated over the whole tank. The dotted line on 26 January mark when the heat was turned back ON.

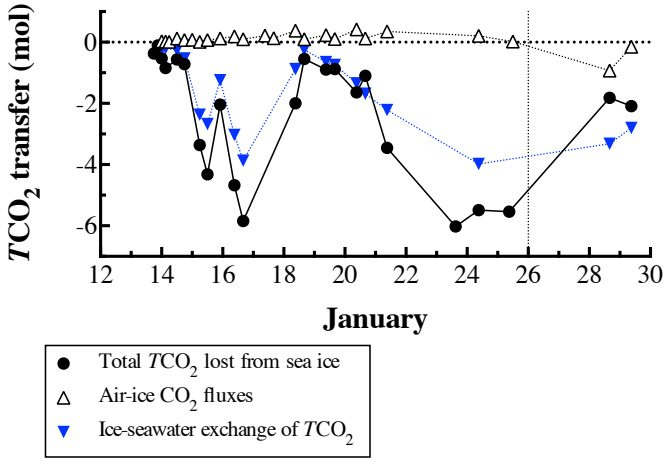

The Cryosphere Discuss., doi:10.5194/tc-2016-14, 2016
Manuscript under review for journal The Cryosphere
Published: 11 February 2016

The Cryosphere Discussions
Open Access
EGU

Figure 10: Evolution of $\Omega_{aragonite}$ in the water column, based on $TA_{(sw)}$ and $TCO_{2(sw)}$ (black dots) and based on $TA_{(sw)}^{*}$ and $TCO_{2(sw)}^{*}$ (dashed red line).